Anatase-to-Rutile Phase Transition in TiO2 Nanoparticles Irradiated by Visible Light

ARTICLE *in* THE JOURNAL OF PHYSICAL CHEMISTRY C · MARCH 2013

Impact Factor: 4.77 · DOI: 10.1021/jp312325h

7 AUTHORS, INCLUDING:

P.C. Ricci
Università degli studi di Cagliari
104 PUBLICATIONS **751** CITATIONS
SEE PROFILE

Luigi Stagi
Università degli studi di Cagliari
14 PUBLICATIONS **45** CITATIONS
SEE PROFILE

Alberto Casu
Istituto Italiano di Tecnologia
44 PUBLICATIONS **497** CITATIONS
SEE PROFILE

Stefano Enzo
Università degli Studi di Sassari
239 PUBLICATIONS **2,806** CITATIONS
SEE PROFILE

THE JOURNAL OF PHYSICAL CHEMISTRY C

Article

pubs.acs.org/JPCC

Anatase-to-Rutile Phase Transition in TiO_2 Nanoparticles Irradiated by Visible Light

Pier Carlo Ricci,*[,†] Carlo Maria Carbonaro,[†] Luigi Stagi,[†] Marcello Salis,[†] Alberto Casu,[‡] Stefano Enzo,[§] and Francesco Delogu[∥]

[†]Dipartimento di Fisica, Università degli Studi di Cagliari, S.P. Monserrato-Sestu Km 0,700, 09042 Monserrato (CA), Italy

[‡]Istituto Italiano di Tecnologia (IIT), via Morego 30, 16163 Genova, Italy

[§]Dipartimento di Chimica e Farmacia, Università degli Studi di Sassari, via Vienna 2, 07100 Sassari, Italy

[∥]Dipartimento di Ingegneria Meccanica, Chimica, e dei Materiali, Università degli Studi di Cagliari, via Marengo 2, 09123 Cagliari, Italy

Supporting Information

ABSTRACT: The light-induced phase transition of TiO_2 nanoparticles from anatase to rutile structure is reported depending on the surrounding environment, the transition being accomplished under oxygen-poor conditions. The transition mechanism is interpreted in the framework of oxygen adsorption and desorption phenomena with the involvement of surface oxygen vacancies and F centers. It is shown that the observed phase transition is not thermally driven because the local temperature of the nanoparticles during irradiation is about 370 K (estimated through the Stokes to anti-Stokes Raman peaks ratio). On the contrary, the phase transition is initiated by intragap irradiation (with the exception of the red light one) that acts as TiO_2 surface sensitizer, promoting the activation of the surface and the nucleation of rutile crystallites starting from two activated anatase neighboring nanoparticles.

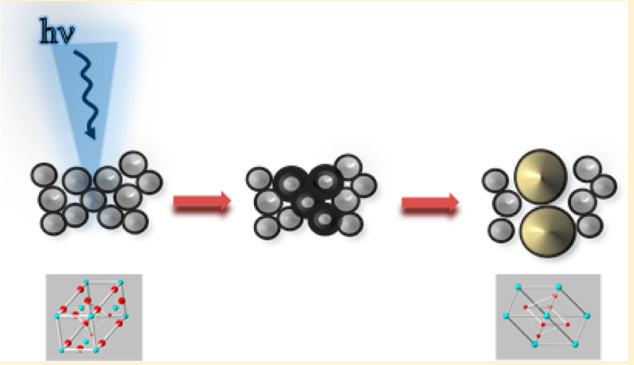

INTRODUCTION

Titanium dioxide (TiO_2) is a semiconductor strategic to a variety of cutting-edge areas of science and engineering, with applications ranging from medicine to chemical and electronic industries.[1−7] It is a polymorphic material with three allotropic forms, namely anatase, brookite, and rutile. Characterized by the highest thermodynamic stability at room temperature and pressure, rutile exhibits a tetragonal $P4_2/mnm$ crystalline structure. Instead, brookite and anatase are respectively orthorhombic *Pbca* and tetragonal $I4_1/amd$. In combination with a high dielectric constant, the large band gap nominates rutile as a natural candidate to semiconductor electronics, where it is actually widely employed. However, anatase attracts as well considerable interest, mostly due to its superior photocatalytic properties.[8]

The physical and chemical properties of rutile, brookite, and anatase are affected by size effects and related surface effects. The size reduction of coherent diffraction domains down to the nanometer range induces, for these TiO_2 systems, a marked change of band gaps and refractive indexes as well as of the rates of charge transfer across interfaces. In turn, this results in enhanced photocatalytic properties[8] in the anatase phase, with important consequences for the photoassisted production of hydrogen from water,[9] and the efficiency of dye-sensitized solar cells.[10,11] The enhancement of photoactivity is even larger for nanometer-sized systems containing different TiO_2 phases,[12] probably due to an effective separation of charge carriers in the different phases, which suppresses the electron−hole recombination mechanism.[12]

Within this framework, achieving a suitable control of the phase transition behavior of nanometer-sized TiO_2 materials would represent a significant progress on the way of their full exploitation in different areas of science and engineering.[12−15] In this regard, it must be noted that also the relative thermodynamic stability of rutile, brookite, and anatase is affected by size effects. In particular, anatase becomes the most stable phase as the size of coherent diffraction domains is smaller than 13−16 nm,[16,17] being the surface energies of rutile and anatase equal to about 1.91 and 1.32 J m^{-2},[16] respectively. Accordingly, the anatase-to-rutile phase transition in nanostructured systems can be induced by raising the temperature above 970 K.[18] Experimental findings suggest that the occurrence of such phase transition is related to the coalescence of neighboring anatase grains at high temperature.[16−20] In addition, the phase transition behavior is affected by the initial grain size, chemical surroundings, and impurities.[16−20]

Received: December 14, 2012
Revised: March 21, 2013
Published: March 22, 2013

Along this line, it has been recently pointed out that the irradiation of nanometer-sized anatase particles is able to influence their stability provided that experiments are performed under suitable incident radiation power and oxygen partial pressure conditions.[21] More specifically, it has been shown that the intragap excitation of anatase particles in an oxygen-rich atmosphere promotes the surface adsorption of O_2 molecules, with a stabilizing effect on the existing oxygen vacancies at the particle surface. On the contrary, when irradiation is performed in vacuum, anatase is transformed into an amorphous TiO_2 phase.

Such evidence clearly demonstrate that irradiation can significantly affect the relative stability of nanometer-sized TiO_2 structures. Focusing on the response of nanometer-sized anatase to irradiation under different powder density and atmosphere conditions, the present work throws new light on the intimate nature of the irradiation effects. It is shown that irradiation is able to induce an athermal anatase-to-rutile phase transition and that the mechanism underlying the phase transition is strictly connected with the chemistry of TiO_2 surfaces.

EXPERIMENTAL SECTION

Samples. Experiments were performed on two sets of anatase powders of different provenience. In the first case, anatase powders were prepared by a conventional sol−gel method involving two steps. Initially, an amorphous xerogel was formed. Afterward, the xerogel was heated at 300 °C for 6 h in oxygen flux to obtain the final powders. In the second case, high-purity anatase dry powders were purchased at Plasmachem (PL-TiO-NO). A set of rutile powders was also purchased at Sigma-Aldrich (634662, particle size <100 nm) to carry out control experiments.

Experiments. X-ray diffraction (XRD) methods were used to estimate the average size of coherent diffraction domains. A Rigaku D-Max diffractometer equipped with a Cu Kα radiation tube, and a graphite monochromator in the diffracted beam, was employed. The XRD patterns were analyzed by using the Rietveld method to quantify the average size and the average strain content of coherent diffraction domains.[24] The anatase powders synthesized by the sol−gel method exhibit an average crystallite size of about 10 nm, whereas for commercial ones the crystallite size is given between 5 and 8 nm (5% standard deviation). XRD estimates are in agreement with high-resolution transmission electron microscopy (HRTEM) observations. These were performed by using a JEOL JEM-2200FS microscope, equipped with a field-emission gun working at an accelerating voltage of 200 kV, a spherical aberration corrector (by CEOS GmbH) of objective lens allowing to reach a spatial resolution of 0.9 Å, and an in-column Omega filter. The samples were prepared by dropping dilute solutions of nanocrystals (NCs) onto carbon-coated ultrathin copper grids. The average size of anatase particles ranges from 8 to 10 nm for synthesized powders and from 4 to 8 nm for commercial ones (5% standard deviation).

Raman scattering measurements were carried out in backscattering geometry by using a triple spectrometer Jobin-Yvon Dilor integrated system and a liquid nitrogen cooled-charge coupled-device detector; the spectral resolution was about 1 cm^{-1}. The measurements were performed at room temperature. The powder samples were irradiated in vacuum (5×10^{-5} Torr) or exposed to different gaseous atmospheres, namely air, oxygen, and argon. The same dispersion and detection system was employed to record the photoluminescence spectra obtained in the visible range. Unless otherwise indicated, the Raman spectra were acquired in the Stokes region.

Laser irradiation experiments and Raman scattering measurements were carried out on 100 mg powder layers about 1 mm thick deposited on a 25 mm^2 sample holder. The powder samples were irradiated with visible light excitation beams of different power in the 1−10 mW range, focused through a 10× objective with 0.25 NA on a surface area of about 2500 μm^2. Since the excitation beam reaches a penetration depth on the order of 10 μm, even if it exhibits negligible absorption only a small fraction of powder is effectively irradiated. The powder samples were irradiated with different excitation laser beams in the visible range, including the 488.0 and 514.5 nm lines of an argon ion laser (Coherent, Innova-90 C), the 632.0 nm line of a He−Ne laser (Spectra-Physics), and the 785 nm of a diode laser (B&WTek).

RESULTS

Raman spectroscopy allows a clear identification of the different TiO_2 crystalline phases. Anatase and rutile crystallize respectively in the tetragonal $I4_1/amd$ and $P4_2/mnm$ space group. Their unit cells contain four and two TiO_2 formula units, respectively. Anatase exhibits six Raman-active modes, namely one A_{1g}, two B_{1g}, and three E_g. Instead, rutile exhibits four Raman-active modes, namely the B_{1g}, E_g, A_{1g}, and B_{2g} ones. The Raman frequencies for bulk structures are 144 (E_g)*, 197 (E_g), 399 (B_{1g})*, 513−519 cm^{-1} (A_{1g} mode superimposed with B_{1g} mode)*, and 639 (E_g)* cm^{-1} for anatase and 143 (B_{1g})*, 447 (E_g)*, 612 (A_{1g})*, and 826 (B_{2g}) cm^{-1} for rutile.[22,23] Asterisks identify the strongest vibrations in Raman spectra collected at room temperature (Figure 1).

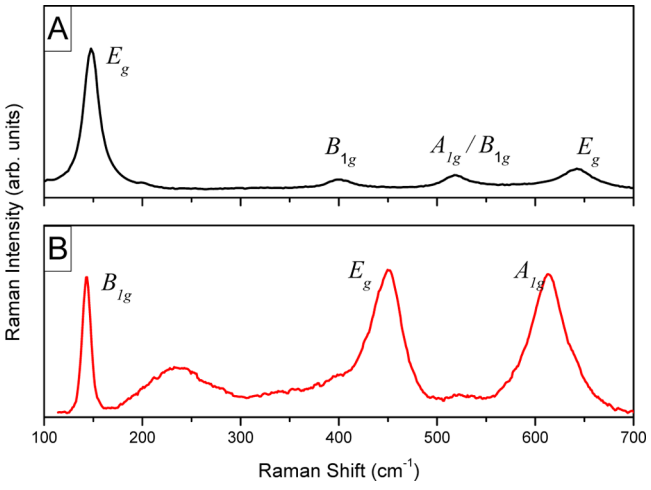

Figure 1. Raman spectra of TiO_2 anatase (A) and rutile (B) nanoparticles.

In a perfect massive crystal, only the phonons closer to the center of the Brillouin zone (BZ) contribute to the inelastic scattering of an incident radiation. Conversely, a larger portion of the BZ is allowed to effectively participate in scattering processes when the crystal is nanometer sized, due to the weakening of the selection rule $q_0 \approx 0$. Therefore, both the position and shape of the bands in the Raman spectra can change. In agreement with the phonon dispersion curve for

dx.doi.org/10.1021/jp312325h | J. Phys. Chem. C 2013, 117, 7850−7857

anatase particles of about 10 nm,[25,26] the Raman spectrum of anatase powders shown in Figure 1A exhibits the main peak of the E_g mode at 148 cm^{-1}. In Figure 1B, the reference spectrum of rutile powders is reported: besides the main vibrational peaks, the typical contribution of the second-order scattering at 238 cm^{-1} is observed.

The effects of irradiation on nanometer-sized anatase particles can be pointed out by comparing Raman spectra collected at increasing times. A representative sequence of such spectra is shown in Figure 2. Data refer to the continuous

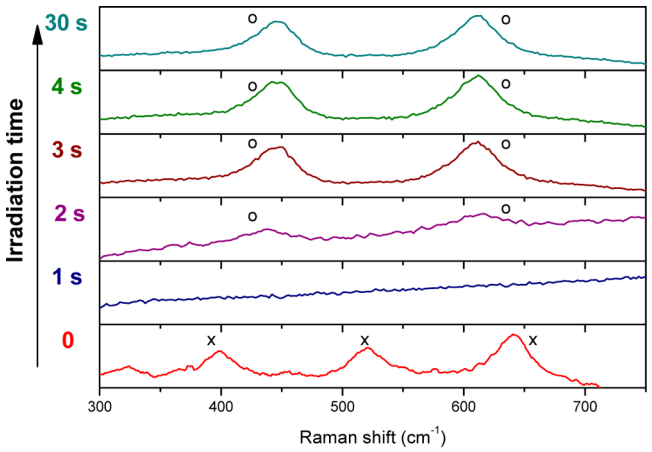

Figure 2. Time evolution of the Raman spectrum of TiO_2 anatase nanoparticles under continuous irradiation at 488.0 nm in vacuum conditions (5×10^{-5} Torr). The spectra were recorded at 5 mW of laser beam power. Zero time spectrum refer to the pristine sample conditions; data were recorded with a time step of 1 s. (×) refer to the anatase phase peaks; (○) refer to the rutile peaks.

irradiation of anatase at a wavelength of 488.0 nm under dynamic vacuum conditions, with a residual pressure on the order of 5×10^{-5} Torr. The Raman spectra were collected in the continuous mode, with a sampling time of 1 s, no time interval between consecutive measurements, and a laser beam power of 5 mW. The measurements were performed within the spectral region between 300 and 700 cm^{-1}, where the highly intense Raman-active vibration modes of anatase and rutile allow the easiest identification of the crystal phase.

It can be seen from Figure 2 that the Raman spectra of irradiated anatase change quickly with time. Initially, the system contains exclusively anatase, as proven by the position of the three peaks at 399, 519, and 639 cm^{-1}. After 1 s, no vibration mode can be identified in the Raman spectrum, which indicates the formation of an amorphous phase. This phase is also characterized by a large and intense photoluminescence (Supporting Information, S1). After 2 s irradiation, two large bands at about 445 and 610 cm^{-1} appear in the Raman spectrum overlapped to a residual photoluminescence background. As the irradiation time increases, the two bands increasingly sharpen, whereas the photoluminescence totally quenches. The presence of two bands at 447 and at 612 cm^{-1} in the final Raman spectra clearly indicates the formation of rutile. The exposure of the powder sample to the laser beam for longer times does not result in further changes. The rutile phase formed in the irradiated region of the sample keeps stable also when exposed to air. In the sample regions not directly exposed to laser irradiation the powder keeps the initial anatase phase independently of the sample holder atmosphere.

Experiments carried out with laser beams of different power indicate the existence of a light power threshold. In particular, the experimental findings suggest that a minimum power of about 1−2 mW is necessary to activate the anatase-to-rutile phase transition for chamber pressure of about 5×10^{-5} Torr. In addition, it appears that the light power does not affect the stability of the rutile phase, which keeps its crystalline structure in vacuum even when the power of the 488.0 nm laser is increased up to 10 mW.

In principle, the observed phase transition could be ascribed to irradiation-induced thermal effects. A similar scenario has been already discussed in the literature for nanometer-sized anatase particles irradiated in air with a high-power laser.[27,28] With the aim of clarifying this issue, the effective temperature of the powder samples during irradiation was estimated by the ratio of the Stokes and anti-Stokes components of the Raman spectrum (Supporting Information, S2). More specifically, the E_g mode of anatase at 148 cm^{-1} and the B_{1g} mode of rutile at 445 cm^{-1} were monitored respectively in air and in vacuum for laser beams with a power as high as 5 mW, i.e., roughly 3−5 times higher than the one needed to activate the observed anatase-to-rutile phase transition. In both cases, the ratio took similar values before and after the sample was irradiated in continuous mode for time intervals as long as 5 min, yielding an estimated temperature of 371 ± 5 K. Being this temperature well below the one required to activate the phase transition,[16,19] the experiments carried out strongly suggest an athermal mechanism for the observed anatase-to-rutile phase transition.

At least three crucial questions arise in connection with the experimental findings heretofore discussed. In the first place, what is the effect of the irradiation wavelength on the observed phase transition? Similarly, what is the effect of the atmosphere to which powders are exposed? Finally, is irradiation needed only to activate the phase transition, or it is necessary to drive the transition?

A response to the latter question has been given on the basis of suitably designed experiments in which irradiation was consecutively switched off and on. The Raman spectra obtained under such conditions are shown in Figure 3. Data refer to

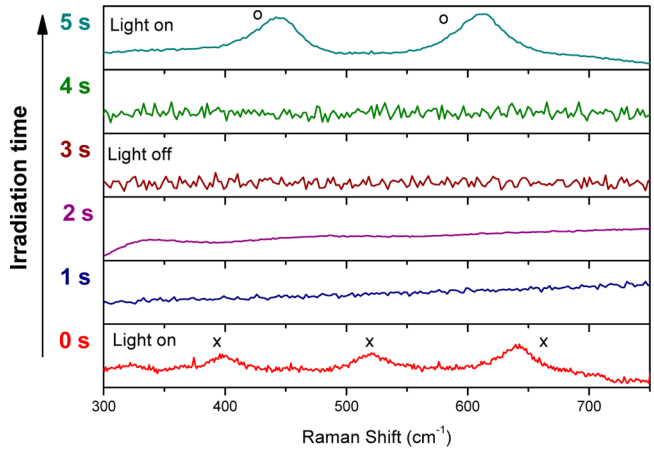

Figure 3. Time evolution of the Raman spectrum of TiO_2 anatase nanoparticles under continuous irradiation at 488.0 nm in vacuum conditions (5×10^{-5} Torr). The spectra were recorded at 10 mW of laser beam power but for the last one recorded at 1 mW. Zero time spectrum refers to the pristine sample conditions; data were recorded with a time step of 1 s. Crosses refer to the anatase phase peaks; circles refer to the rutile peaks.

dx.doi.org/10.1021/jp312325h | J. Phys. Chem. C 2013, 117, 7850−7857

experiments carried out under dynamic vacuum conditions, with a residual pressure of about 5×10^{-5} Torr and a laser beam power of 10 mW. A time of 1 s laser irradiation suffices to induce the transformation of the anatase into an amorphous phase. When irradiation is switched off after 2 s, only a flat zero dark signal is detected. As soon as the irradiation light is switched on again, after a total of 4 s, the amorphous phase is replaced by rutile. In this case, the rutile phase forms quickly, and no significant evolution in its Raman spectrum is observed. It is also worth noting that the formation of rutile was monitored by using a very low power laser beam of 1 mW. These results strongly suggest that the rutile phase does not form during the irradiation period, but rather as a consequence of irradiation. Correspondingly, it seems reasonable to associate irradiation exclusively with an activation stage of the anatase-to-rutile phase transition.

In order to explore the effects of the irradiation wavelength on the phase transition behavior, irradiation experiments at 514.5, 632.8, and 785.0 nm intrinsic excitation wavelengths were carried out. The irradiation of anatase powders with the 514.5 nm wavelength gives rise to the same experimental scenario already discussed for the laser irradiation at 488.0 nm. Conversely, irradiation in the red and near-infrared spectral regions is unable to induce the anatase-to-rutile phase transition (Supporting Information, S3).

Finally, the role of the atmosphere to which anatase is exposed during irradiation was investigated by performing experiments under different conditions, namely in oxygen and argon ambient. In oxygen, irradiation is unable to activate any phase transition. Correspondingly, anatase keeps stable up to an excitation power of 10 mW, well above the power threshold required to induce the anatase-to-rutile phase transition at low pressure. Moreover, apparently irradiation reduces or suppresses the initial photoluminescence background (Supporting Information, S4).

The results of the Raman measurements performed in argon are shown in Figure 4. In this case, the system exhibits the same phase transition trend observed under vacuum conditions.

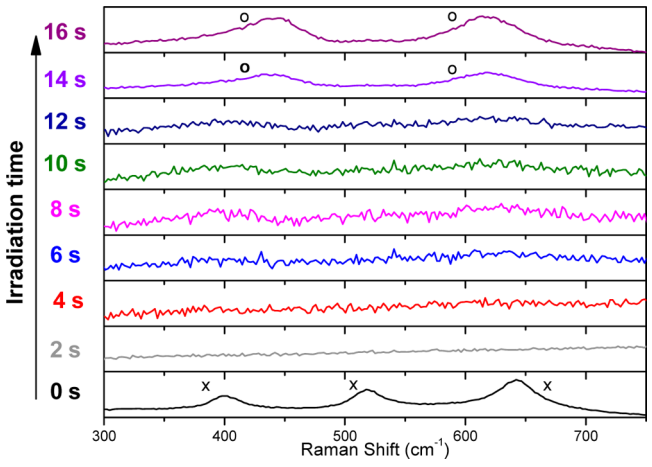

Figure 4. Time evolution of the Raman spectrum of TiO_2 anatase nanoparticles under continuous irradiation at 488.0 nm in an argon atmosphere. The spectra were recorded at 10 mW of laser beam power. Zero time spectrum refers to the pristine sample conditions; data were recorded with a time step of 2 s. Crosses refer to the anatase phase peaks; circles refer to the rutile peaks.

However, the phase transition requires quite longer times to take place, reaching completion after 14 s.

These experimental findings suggest a definite role in the mechanistic processes underlying the phase transition for the chemical interactions at the surface of the nanometer-sized anatase particles. To further investigate this feature, attention was focused on the irradiation behavior of commercial anatase powders that have undergone surface passivation by treatment with a concentrated nitric acid aqueous solution.

The Raman spectrum of the surface-passivated anatase samples in air is shown in Figure 5A. The typical vibration modes of anatase at 154.5, 456, 519, and 617 cm^{-1} can be readily identified, although the position of the different bands and their half-maximum full width are affected by phonon confinement effects.[25,29] An additional band at 1050 cm^{-1}, originated by the $\nu\nu$(NO) vibration mode of the NO_3^- groups bonded at the surface,[30] can be also identified.

Irradiation experiments point out that the surface-passivated anatase is more resistant than anatase to irradiation effects. The Raman spectra in Figure 5B indicate that, in argon and under dynamic vacuum conditions, the anatase-to-rutile phase transition is partially inhibited and/or takes place after longer irradiation times.

In addition, the phase transition only takes place when the power of the irradiating laser is as high as 5−6 mW. Furthermore, the time evolution underlying the effective phase formation (anatase, intermediate amorphous phase, rutile) drastically changes from point to point in the sample. As a consequence, we observed the appearance of regions in which anatase and rutile phases are mixed, as shown by the Raman spectrum in Figure 5D.

In this respect, it must be noted that the Raman spectrum of the regions containing anatase still exhibits the vibration band at 1050 cm^{-1} due to the surface passivation with nitric acid. On the contrary, the $\nu\nu$(NO) vibration mode is no longer present in the Raman spectra of the regions containing only rutile (Figure 5C). This is a further strong indication that the surface of the anatase particles plays a fundamental role in the phase transition trend.

The effects of the passivating nitric groups at the surface of the surface-passivated anatase particles were qualitatively assessed by studying the phase transition behavior of surface-passivated anatase particles in which the surface nitric groups were removed. To such aim, surface-passivated anatase powders were kept at 80 °C under vacuum conditions for several hours, a time sufficient to obtain the total suppression of the band at 1050 cm^{-1} in the Raman spectrum. When irradiated in vacuum and argon, the obtained anatase samples underwent a fast anatase-to-rutile phase transition. In agreement with previous measurements, no phase transition was observed when the samples were irradiated in oxygen or air.

Additional information on the anatase-to-rutile phase transition was gained by XRD and HRTEM analyses. In the former case, the XRD patterns of powder samples irradiated under dynamic vacuum conditions exhibit relatively weak peaks overlapping the intense anatase ones that can be ascribed to the presence of a rutile phase diluted in an anatase matrix (Supporting Information, S5). In the light of the very small volume of anatase effectively irradiated by the laser beams, the low intensity of the rutile XRD peaks can be exclusively related to the very small amount of rutile present in the sample compared with anatase. The Rietveld analysis of the XRD patterns indicates that the coherent diffraction domains of the

dx.doi.org/10.1021/jp312325h | J. Phys. Chem. C 2013, 117, 7850−7857

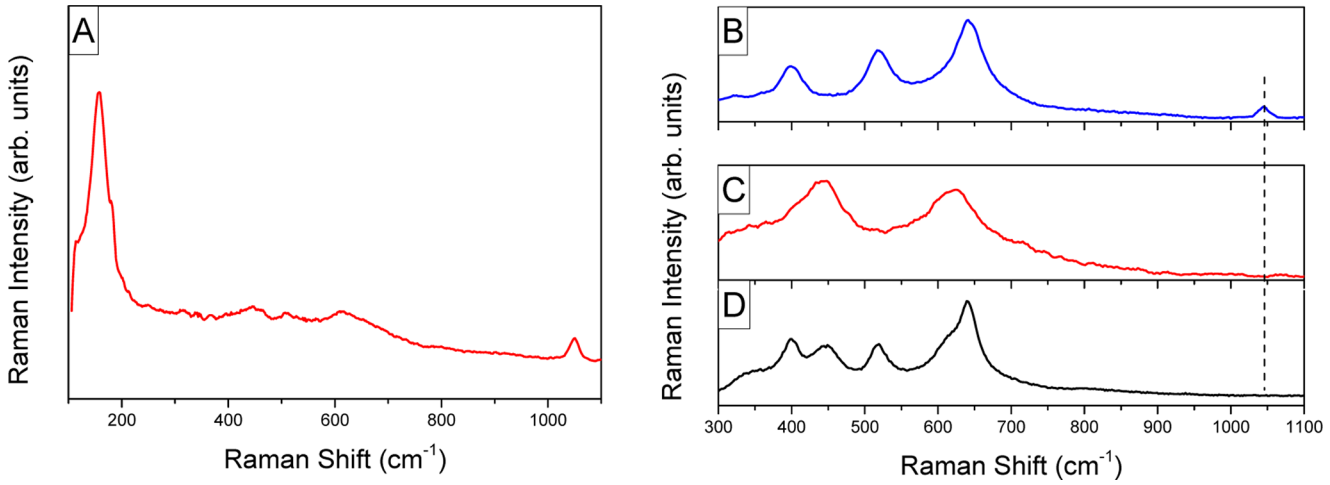

Figure 5. (A) Anatase spectrum recorded in air. (B–D) Point-dependent Raman spectra of the surface-passivated anatase nanopowders after irradiation in vacuum. Dashed line marks the $\nu\nu$(NO) vibration mode of the NO_3^- groups bonded at the surface.

starting anatase exhibit an average size of about 10 nm, whereas this quantity increases up to about 100 nm for the rutile phase formed by irradiation.

Figure 6A displays a HRTEM image of representative untreated TiO_2 NCs of less than 10 nm in size. As expected, the

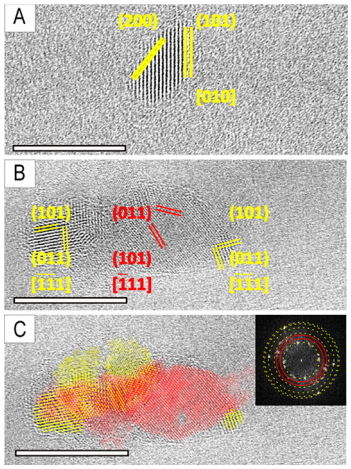

Figure 6. (A) HRTEM image of a TiO_2 NC with anatase crystal structure observed along the [010] zone axis, exhibiting (101) and (200) lattice sets with measured *d*-spacings of 3.51 and 1.89 Å. (B) HRTEM of a TiO_2 aggregate featuring NCs of rutile and anatase. The rutile NC, observed along the [−111] zone axis (center, in red), exhibits (101) and (011) lattice sets with measured *d*-spacings of 3.19 Å; anatase NCs, observed along the [−1−1−1] zone axis (left and right, in yellow), exhibit (101) and (011) lattice sets with measured *d*-spacings of 3.51 Å. (C) Reconstruction via inverse fast Fourier transform (IFFT) of the NCs forming the aggregate of point (B): rutile and anatase NCs are depicted in red and in yellow, respectively. The inset features the FFT pattern of the aggregate. Red lines and yellow dotted lines indicate spots of rutile and anatase phase, respectively. All the data bars correspond to 10 nm.

NCs, showing elongated shapes, exhibit the lattice sets of anatase, and their size is in accordance with XRD analysis. A HRTEM image of the treated TiO_2 sample showing a small polycrystalline aggregate is reported in Figure 6B. Lattice fringes show *d*-spacing and spatial relationships of two different phases, namely anatase (JCPDS card 84-1286) and rutile (JCPDS card 82-0514); the bidimensional Fourier transform (2D_FT) pattern of the TiO_2 aggregate features contributions arising from different NCs, which were identified and discerned by angular and vector relationships among the spots of reciprocal lattice (inset of Figure 6C). The aggregate can subsequently be "broken down" into its nanocrystalline parts and reconstructed as an inverse Fourier transform, where multiple rutile and anatase NCs are identified by different false colors (Figure 6C). The presence of rutile in relatively large aggregates was also ascertained by side-aperture electron diffraction (SAED) analyses. A representative pattern is shown in Supporting Information, S6.

DISCUSSION AND MODELING

According to the experimental evidence previously discussed, the irradiation-induced anatase-to-rutile phase transition can be ascribed to chemical processes occurring at the surface of nanometer-sized anatase particles. It can be reasonably expected that the athermal mechanism underlying the phase transition relies upon the generation of surface defects due to optical excitation and their subsequent interaction with the chemical surroundings.

In this respect, it is well-known that irradiation can have quite different effects on nanometer-sized TiO_2 systems depending on the atmosphere surrounding the sample. For example, the irradiation of nanometer-sized anatase particles in air with a laser beam of high power results in a significant increase of their degree of crystalline order.[31] Also, it was shown that the crystalline phase of anatase nanoparticles can be deteriorated down to an amorphous phase through irradiation at low power density laser beam under vacuum conditions.[21] In both cases, the absorption and desorption of oxygen molecules on the surface of nanometer-sized TiO_2 systems are expected to play a fundamental role.

When absorbed on the surface, the oxygen molecules are known to behave as efficient electron scavengers. They are able to collect electrons excited from the surface states of the semiconductor to the conduction band and partially compensate for the effects of oxygen vacancies.[32−34] As suggested by X-ray photoelectron spectroscopy studies,[35,36] these are responsible for the formation of Ti^{3+} and Ti^{4+} ions as a consequence of electron trapping effects.[33] The absorbed oxygen molecules are expected to stabilize the structure of the TiO_2 surface by bridging two neighboring Ti sites.[32]

dx.doi.org/10.1021/jp312325h | J. Phys. Chem. C 2013, 117, 7850−7857

The desorption of the oxygen molecules absorbed at the TiO_2 surface has been connected with the recombination of the electrons trapped in the monovalent anionic oxygen molecules with the holes in the photoexcited valence band.[32,37,38] Recently, it has been proposed that this photodesorption mechanism must also operate under intrinsic excitation conditions, i.e., when the holes involved in the recombination process underlying the desorption of oxygen molecules derive from charged F centers generated in correspondence of oxygen vacancies.[21,32] It follows that the electronic excitation of nanometer-sized anatase particles is able to promote both the adsorption and the desorption of oxygen molecules at the particle surface.[21] The relative balance between the two processes will depend on the experimental conditions,[21,39] as confirmed by the results reported in Figures 2−4. It can be easily inferred that irradiation in an oxygen-poor atmosphere, i.e., under dynamic vacuum conditions or in argon, will result in the excitation of the electrons in the conduction band. In turn, this will induce the desorption of oxygen molecules and a depletion of oxygen atoms at the surface of the nanometer-sized anatase particles. As the power of the laser beam increases, the number of excited electrons also increases, with a beneficial effect on the rate of the oxygen desorption.

According to ref 21, the increasing of the excitation power on the TiO_2 anatase nanoparticles in an oxygen-poor atmosphere (that is, under dynamic vacuum conditions or in an argon-rich environment) generates a high electron density in the conduction band and a rapid depletion of oxygens at the nanoparticle's surface. In this scenario, we reckon that the irradiation-induced desorption of oxygen molecules leaves the particle's surface highly reactive. The enhanced chemical reactivity of these surfaces favors the mutual interactions of neighboring particles, which finally determine the formation of stable polycrystalline aggregates. For example, the chemical decomposition of peroxyl groups at the particle surface can permit to neighboring particles the formation of stable interparticle chemical bonds.[40−42]

The size increase of the coherent diffraction domains of rutile can be regarded as an indication of the above-mentioned aggregation mechanism in the starting anatase powder. Rutile nucleates as a consequence of the irradiation-induced desorption of oxygen molecules from the surface of anatase particles. Under pulsed laser ablation conditions, nanometer-sized anatase particles exhibit a tendency to coalesce at {112} surfaces, forming faulted and twinned bicrystals that can act as preferential nucleation sites for the rutile phase.[43] Molecular dynamics calculations employing suitable reactive force fields, as well as *in situ* TEM observations, pointed out that the first stage of the thermally induced anatase-to-rutile phase transition in nanometer-sized particles consists in the formation of chemical bonds between amorphous and defective surfaces.[44−46] In a second stage, the rutile phase nucleates exactly at the twin boundaries generated by anatase {112} surfaces.[45,46]

The relative number of preferential nucleation sites for the anatase-to-rutile phase transition increases as the size of anatase particles decreases and as the population of oxygen vacancies at the particle surface increases.[47,48] Once nucleated, the rutile phase undergoes a fast growth, absorbing the neighboring anatase domains into a single coherent crystalline lattice.[44,48,49] The transformation of bulk anatase breaks out 7 of the 24 Ti−O bonds per unit cell leading to the cooperative displacement of both Ti and O atoms. The growth of the coherent rutile domain terminates at the anatase surfaces different from the {112} one or at the interface with another rutile domain.[44,48]

It is worth pointing out that in ref 21 the anatase-to-rutile phase transition was not observed, whereas only the degradation of the pristine anatase phase to an amorphous phase was reported. Those experiments were carried out at very low power density laser beam, fixing the excitation wavelength at 488 nm. The maximum power density delivered at the sample was 4 W/cm^2 (about 1/10th of the estimated power density threshold to achieve the anatase to rutile phase transition). In addition, the final irradiation was reached in steps of 0.5 W/cm^2 for prolonged time. In that condition, the rate of the formation of the surface defects being very slow, we retain that the lattice has the possibility for a partial rearrangement. On the contrary, in the present experimental conditions, where a larger power density was delivered at the sample, a high and fast increase of the concentration of surface defects can be reached (at an estimated power density threshold of 40 W/cm^2), leading to nanoparticles' surfaces very reactive which favor the mutual interactions between neighboring particle and the formation of stable polycrystalline aggregates.

The experimental findings regarding the phase transition behavior of surface-passivated anatase particles are consistent with the above-mentioned mechanistic scenario. As far as the particle surface is functionalized by chemically bonded nitric groups, the phase transition is strongly inhibited. Only once the nitric groups are removed, irradiation is able to enhance the chemical reactivity of the surface.

These results are also consistent with the experimental evidence regarding the behavior of nanometer-sized anatase particles with a thin shell La_2O_3 at the surface.[49,50] In this case, the direct contact between the anatase crystals in neighboring particles is prevented by the La_2O_3 shell.[50] Correspondingly, the anatase-to-rutile phase transition is significantly hindered or even completely prevented.[50]

A further support to the above-mentioned mechanism comes from the irradiation-induced phase transition behavior of carbon-rich anatase in air.[51] In this case, irradiation induces the formation of gaseous carbon monoxide and carbon dioxide molecules, determining the formation of a large number of oxygen vacancies at the particle surface.[46] This enables the occurrence of the anatase-to-rutile phase transition. On the contrary, irradiation is not able to increase the concentration of oxygen vacancies at the surface of carbon-free anatase particles, and the phase transition no longer occurs irrespective of the power used in irradiation experiments.[51] Being these evidence referred to experiments performed in air, the results are in agreement with the novel experimental findings obtained in the present work.

Finally, it is worth noting that the transformation in rutile is not simultaneous to the light irradiation and is not connected to the simultaneous heating of the sample, but it takes place after the excitation process. This fact evidences the role of the light as a sensitizer of surface agglomerations while the phase transition is connected to structural dynamics and to the role of anatase surface defects and twins. In this scenario the role of surface species or, in general, the defects density on the surface of the nanoparticles plays a key role in the anatase-to-rutile phase transition. For this reason focalized measurements on the defects properties as a function of the synthesis conditions, pre- and post-treatment procedures, and surface passivation is

mandatory for a full comprehension of the observed light-induced phase transition process.

CONCLUSIONS

The irradiation of nanometer-sized anatase particles with visible light induces the anatase-to-rutile phase transition provided that experiments are performed in vacuum or in an argon atmosphere. No phase transition occurs in air or in oxygen atmospheres or when radiation with wavelength in the red and near-infrared spectral regions is used. For the phase transition to take place, the power of irradiation must also be higher than a minimum threshold. The phase transition is governed by an athermal mechanism connected with the interaction of the particle surface with the chemical surroundings. In particular, the electron excitation processes activated by irradiation affect the rate of absorption and desorption of oxygen molecules, which in turn can be related to the number of oxygen vacancies at the particle surface. In the absence of gaseous oxygen, the electronic excitation determines a predominance of the oxygen desorption processes. These induce a significant enhancement of the surface chemical reactivity, which results in the formation of stable chemical bonds between the surfaces of neighboring anatase particles. Such regions are likely to represent the preferential sites for the nucleation of rutile. Whereas irradiation is necessary to activate the formation of the first nuclei of rutile, their growth can be ascribed to atomistic processes set on activated surfaces, the irradiation acting as the surface sensitizer.

ASSOCIATED CONTENT

Supporting Information

Photoluminescence spectrum of TiO_2 nanoparticles recorded during laser irradiation; calculation of the effective temperature on the nanopowder during irradiation; Raman spectra of TiO_2 anatase nanoparticles under irradiation at different wavelength in vacuum conditions (5×10^{-5} Torr); Raman spectrum of TiO_2 anatase nanoparticles under continuous irradiation at 488.0 nm in an oxygen atmosphere (excitation power of 10 mW); XRD diffraction pattern of treated nanoparticles; SAED pattern and HRTEM image of treated TiO_2 nanoparticles. This material is available free of charge via the Internet at http://pubs.acs.org.

AUTHOR INFORMATION

Corresponding Author

*E-mail carlo.ricci@dsf.unica.it.

Notes

The authors declare no competing financial interest.

ACKNOWLEDGMENTS

The University of Cagliari and the University of Sassari are gratefully acknowledged for the financial support. L.S. gratefully acknowledges Sardinia Regional Government for the financial support of his PhD scholarship (P.O.R. Sardegna F.S.E. Operational Programme of the Autonomous Region of Sardinia, European Social Fund 2007-2013 - Axis IV Human Resources, Objective l.3, Line of Activity l.3.1.).

REFERENCES

(1) Tennakone, K.; Kumara, G. R. R. A.; Kottegoda, I. R. M.; Perera, V. P. S.; Weerasundara, P. S. R. S. Sensitization of Nano-porous Films of TiO_2 with Santalin (Red Sandalwood Pigment) and Construction of Dye-Sensitized Solid-State Photovoltaic Cells. *J. Photochem. Photobiol., A* **1998**, *117*, 137−142.

(2) Long, H.; Chen, A.; Yang, G.; Li, Y.; Lu, P. Third-Order Optical Nonlinearities in Anatase and Rutile TiO_2 Thin Films. *Thin Solid Films* **2009**, *517*, 5601−5604.

(3) Golego, N.; Studenikin, S. A.; Cocivera, M. Sensor Photoresponse of Thin-Film Oxides of Zinc and Titanium to Oxygen Gas. *J. Electrochem. Soc.* **2000**, *147*, 1592−1594.

(4) Page, K.; Palgrave, R. G.; Parkin, I. P.; Wilson, M.; Savin, S. L. P.; Chadwick, A. V. Titania and Silver-Titania Composite Films on Glass-Potent Antimicrobial Coatings. *J. Mater. Chem.* **2007**, *17*, 95−104.

(5) Li, Q.; Mahendra, S.; Lyon, D. Y.; Brunet, L.; Liga, M. V.; Li, D.; Alvarez, P. J. J. Antimicrobial Nanomaterials for Water Disinfection and Microbial Control: Potential Applications and Implications. *Water Res.* **2008**, *42*, 4591−4602.

(6) Wagemaker, M.; Borghols, W. J. H.; Mulder, F. M. Large Impact of Particle Size on Insertion Reactions. A Case for Anatase Li_xTiO_2. *J. Am. Chem. Soc.* **2007**, *129*, 4323−4327.

(7) Deng, D.; Kim, M. G.; Lee, J. Y.; Cho, K. Green Energy Storage Materials: Nanostructured TiO_2 and Sn-Based Anodes for Lithium-Ion Batteries. *J. Energy Environ. Sci.* **2009**, *2*, 818−837.

(8) Carp, O.; Huisman, C. L.; Reller, A. Photoinduced Reactivity of Titanium Dioxide. *Prog. Solid State Chem.* **2004**, *32*, 33−177.

(9) Ni, M.; Leung, M. K. H.; Leung, D. Y. C.; Sumathy, K. A Review and Recent Developments in Photocatalytic Water-Splitting Using TiO_2 for Hydrogen Production. *Renewable Sustainable Energy Rev.* **2007**, *11*, 401−425.

(10) Dürr, M.; Schmidt, A.; Obermaier, M.; Rosselli, S.; Yasuda, A.; Nelles, G. Low Temperature Fabrication of Dye-Sensitized Solar Cells by Transfer of Composite Porous Layers. *Nat. Mater.* **2005**, *4*, 607−611.

(11) Bledowski, M.; Wang, L.; Ramakrishnan, A.; Khavryuchenko, O. V.; Khavryuchenko, V. D.; Ricci, P. C.; Strunk, J.; Cremer, T.; Kolbeck, C.; Beranek, R. Visible-Light Photocurrent Response of TiO_2-Polyheptazine Hybrids: Evidence for Interfacial Charge-Transfer Absorption. *Phys. Chem. Chem. Phys.* **2011**, *13*, 21511−21519.

(12) Ohno, T.; Tokieda, K.; Higashida, S.; Matsumura, M. Synergism Between Rutile and Anatase TiO_2 Particles in Photocatalytic Oxidation of Naphthalene. *Appl. Catal.* **2003**, *244*, 383−391.

(13) Kraleva, E.; Saladino, M. L.; Matassa, R.; Caponetti, E.; Enzo, S.; Spojakina, A. Phase Formation in Mixed TiO_2-ZrO_2 Oxides Prepared by Sol-Gel Method. *J. Struct. Chem.* **2001**, *52*, 330−339.

(14) Wang, J. A.; Limas-Ballesteros, R.; Lopez, T.; Moreno, A.; Gomez, R.; Novaro, O.; Bokhimi, X. Quantitative Determination of Titanium Lattice Defects and Solid-State Reaction Mechanism in Iron-Doped TiO_2 Photocatalysts. *J. Phys. Chem. B* **2001**, *105*, 9692−9698.

(15) Ardizzone, S.; Bianchi, C. L.; Cappelletti, G.; Gialanella, S.; Pirola, C.; Ragaini, V. Tailored Anatase/Brookite Nanocrystalline TiO_2. The Optimal Particle Features for Liquidand Gas-Phase Photocatalytic Reactions. *J. Phys. Chem. C* **2007**, *111*, 13222−13231.

(16) Zhang, H.; Banfield, J. F. Thermodynamic Analysis of Phase Stability of Nanocrystalline Titania. *J. Mater. Chem.* **1998**, *8*, 2073−2076.

(17) Zhang, H.; Banfield, J. F. Understanding Polymorphic Phase Transformation Behavior during Growth of Nanocrystalline Aggregates: Insights from TiO_2. *J. Phys. Chem. B* **2000**, *104*, 3481−3487.

(18) Hwu, Y.; Yao, Y. D.; Cheng, N. F.; Tung, C. Y.; Lin, H. M. X-Ray Adsorption of Nanocrystal TiO_2. *Nanostruct. Mater.* **1997**, *9*, 355−358.

(19) Hanaor, D. A. H.; Sorrell, C. C. Review of Anatase to Rutile Phase Transformation. *J. Mater. Sci.* **2011**, *46*, 855−874.

(20) Barnard, A. S.; Curtiss, L. A. Prediction of TiO_2 Nanoparticle Phase and Shape Transitions Controlled by Surface Chemistry. *Nano Lett.* **2005**, *5*, 1261−1266.

(21) Ricci, P. C.; Casu, A.; Salis, M.; Corpino, R.; Anedda, A. Optically Controlled Phase Variation of TiO_2 Nanoparticles. *J. Phys. Chem. C* **2010**, *114*, 14441−14445.

(22) Ohsaka, T.; Izumi, F.; Fujiki, Y. Raman Spectrum of Anatase TiO_2. *J. Raman Spectrosc.* **1978**, *7*, 321−324.

(23) Mazza, T.; Barborini, E.; Piseri, P.; Milani, P.; Cattaneo, D.; Bassi, A. L.; Bottani, C. E.; Ducati, C. Raman Spectroscopy Characterization of TiO_2 Rutile Nanocrystals. *Phys. Rev. B* **2007**, *75*, 1−5.
(24) Lutterotti, L.; Ceccato, R.; Dal Maschio, R.; Pagani, E. Quantitative Analysis of Silicate Glass in Ceramic Materials by the Rietveld Method. *Mater. Sci. Forum* **1998**, *278*−*281*, 87−90.
(25) Salis, M.; Ricci, P. C.; Anedda, A. An Analytical Form for the Raman Shift Dependence on Size of Nanocrystals. *J. Raman Spectrosc.* **2009**, *40*, 64−66.
(26) Ricci, P. C.; Salis, M.; Anedda, A. Phonon Characterization of Nano-Crystals by Raman Spectroscopy. *Chem. Phys. Lett.* **2008**, *457*, 191−193.
(27) Lee, H.-Y.; Lan, W.-L.; Tseng, T. Y.; Hsu, D.; Chang, Y.-M.; Lin, J. G. Optical Control of Phase Transformation in Fe-Doped TiO_2 Nanoparticles. *Nanotechnology* **2009**, *20*, 315702−315707.
(28) Parussulo, A. L. A.; Huila, M. F. G.; Araki, K.; Toma, H. E. N_3-Dye-Induced Visible Laser Anatase-to-Rutile Phase Transition on Mesoporous TiO_2 Films. *Langmuir* **2011**, *27*, 9094−9099.
(29) Sahoo, S.; Arora, A. K.; Sridharan, S. Raman Line Shapes of Optical Phonons of Different Symmetries in Anatase TiO_2 Nanocrystals. *J. Phys. Chem. C* **2009**, *113*, 16927−16933.
(30) Huang, S.-J.; Walters, A. B.; Vannice, M. A. Adsorption and Decomposition of NO on Lanthanum Oxide. *J. Catal.* **2000**, *192*, 29−47.
(31) Lottici, P. P.; Bersani, D.; Braghini, M.; Montenero, A. Raman Scattering Characterization of Gel-Derived Titania Glass. *J. Mater. Sci.* **1993**, *28*, 177−183.
(32) Klabunde, K. J.; Stark, J.; Koper, O.; Mohs, C.; Park, D. G.; Decker, S.; Jiang, Y.; Lagadic, I.; Zhang, D. Nanocrystals as Stoichiometric Reagents with Unique Surface Chemistry. *J. Phys. Chem.* **1996**, *100*, 12142−12153.
(33) Komaguchi, K.; Maruoka, T.; Nakano, H.; Imae, I.; Ooyama, Y.; Harima, Y. Electron-Transfer Reaction of Oxygen Species on TiO_2 Nanoparticles Induced by Sub-Band-Gap Illumination. *J. Phys. Chem C.* **2010**, *114*, 1240−1245.
(34) Zhou, S. Q.; Cizmar, E.; Potzger, M. K.; Krause, M.; Talut, G.; Helm, M.; Fassbender, J.; Zvyagin, S. A.; Wosnitza, J.; Schmidt, H. Origin of Magnetic Moments in Defective TiO_2 Single Crystals. *Phys. Rev. B* **2009**, *79*, 113201−113205.
(35) Guillot, J.; Fabreguette, F.; Imhoff, L.; Heintz, O.; Marco de Lucas, M. C.; Sacilotti, M.; Domenichini, B.; Bourgeois, S. Amorphous TiO_2 in LP-OMCVD TiN_xO_y Thin Films Revealed by XPS. *Appl. Surf. Sci.* **2001**, *177*, 268−271.
(36) Beranek, R.; Kisch, H. Tuning the Optical and Photoelectrochemical Properties of Surface-Modified TiO_2. *Photochem. Photobiol.* **2007**, *7*, 40−48.
(37) Xiong, L.-B.; Li, J.-L.; Yang, B.; Yu, Y. Ti^{3+} in the Surface of Titanium Dioxide: Generation, Properties and Photocatalytic Application. *J. Nanomater.* **2012**, *2012*, 831524−831537.
(38) Fujishima, A.; Rao, T. N.; Tryk, D. A. Titanium Dioxide Photocatalysis. *J. Photochem. Photobiol., C* **2000**, *1*, 1−21.
(39) Salis, M.; Ricci, P. C.; Anedda, A. Thermodynamics of Optically Assisted Desorption of Oxygen from TiO_2 Nanoparticle Surface. *J. Non-Equilib. Thermodyn.* **2012**, DOI: 10.1515/jnetdy-2011-0033.
(40) Nakamura, R.; Nakato, Y. Primary Intermediates of Oxygen Photoevolution Reaction on TiO_2 (Rutile) Particles, Revealed by In Situ FTIR Absorption and Photoluminescence Measurements. *J. Am. Chem. Soc.* **2004**, *126*, 1290−1298.
(41) Mattioli, G.; Filippone, F.; Bonapasta, A. A. Reaction Intermediates in the Photoreduction of Oxygen Molecules at the (101) TiO_2 (Anatase) Surface. *J. Am. Chem. Soc.* **2006**, *128*, 13772−13780.
(42) Ulmann, M.; De Tacconi, N. R.; Augustynski, J. Behavior of Surface Peroxo Species in the Photoreactions at TiO_2. *J. Phys. Chem.* **1986**, *90*, 6523−6530.
(43) Tsai, M.-H.; Shen, P.; Chen, S.-Y. Defect Generation of Anatase Nanocondensates Via Coalescence and Transformation from Dense Fluorite-Type TiO_2. *J. Appl. Phys.* **2006**, *100*, 114313−114319.
(44) Zhou, Y.; Fichthorn, K. A. Microscopic View of Nucleation in the Anatase-To-Rutile Transformation. *J. Phys. Chem. C* **2012**, *116*, 8314−8321.
(45) Penn, R. L.; Banfield, J. F. Formation of Rutile Nuclei At Anatase {112} Twin Interfaces and the Phase Transformation Mechanism in Nanocrystalline Titania. *Am. Mineral.* **1999**, *84*, 871−876.
(46) Zhang, J.; Xu, Q.; Li, M.; Feng, Z.; Li, C. UV Raman Spectroscopic Study on TiO_2. II. Effect of Nanoparticle Size on the Outer/Inner Phase Transformations. *J. Phys. Chem. C* **2009**, *113*, 1698−1704.
(47) Rath, C.; Mohanty, P.; Pandey, A. C.; Mishra, N. C. Oxygen Vacancy Induced Structural Phase Transformation in TiO_2 Nanoparticles. *J. Phys. D: Appl. Phys.* **2009**, *42*, 205101−205107.
(48) Li, X.; Quan, X.; Kutal, C. Synthesis and Photocatalytic Properties of Quantum Confined Titanium Dioxide Nanoparticle. *Scr. Mater.* **2004**, *50*, 499−505.
(49) Gouma, P. I.; Dutta, P. K.; Mills, M. J. *Nanostruct. Mater.* **1999**, *11*, 1231−1237.
(50) Zhang, J.; Li, M.; Feng, Z.; Chen, J.; Li, C. UV Raman Spectroscopic Study on TiO_2. I. Phase Transformation at the Surface and in the Bulk. *J. Phys. Chem. B* **2006**, *110*, 927−935.
(51) Chatterjee, A.; Wu, S.-B.; Chou, P.-W.; Wong, M. S.; Cheng, C.-L. Observation of Carbon-Facilitated Phase Transformation of Titanium Dioxide Forming Mixed-Phase Titania by Confocal Raman Microscopy. *J. Raman Spectrosc.* **2011**, *42*, 1075−1080.